INT. J. NUM. METH. HEAT FLUID FLOW, VOL. 5, 13–33 (1995)

NUMERICAL EXPERIMENTS IN TURBULENT NATURAL AND MIXED CONVECTION IN INTERNAL FLOWS

C. D. PÉREZ-SEGARRA, A. OLIVA, M. COSTA AND F. ESCANES

Laboratori de Termotècnia i Energètica, Dept. Màquines i Motors Tèrmics, Universitat Politècnica de Catalunya, C/Colom 9, E-08222 Terrassa, Barcelona, Spain

ABSTRACT

In this paper a numerical simulation, based on finite difference techniques, has been developed in order to analyse turbulent natural and mixed convection of air in internal flows. The study has been restricted to two-dimensional cavities with the possibility of inlet and outlet ports, and with internal heat sources. Turbulence is modelled by means of two-equation k-ε turbulence models, both in the simplest form using wall functions and in the more general form of low-Reynolds-number k-ε models. The couple time average governing equations (continuity, momentum, energy, and turbulence quantities) are solved in a segregated manner using the SIMPLEX method. An implicit control volume formulation of the differential equations has been employed. Some illustrative numerical results are presented to study the influence of geometry and boundary conditions in cavities. A comparison of different k-ε turbulence models has also been presented.

KEY WORDS Natural convection Mixed convection Turbulence k-ε model

NOMENCLATURE

c_p	specific heat at constant pressure
$c_{\varepsilon 1}$, $c_{\varepsilon 2}$, $c_{\varepsilon 3}$,	empirical constants in the turbulence
c_μ, c_1, c_θ	models
CV	control volume
D, E	extra terms in the k and ε equations
f_1, f_2, f_μ	empirical functions in the turbulent models
g	gravitational acceleration
G_k	buoyancy production/destruction of k
H, H_1,.....	vertical distances (see Fig. 1)
k	turbulent kinetic energy
k_x k_y	concentration factors in x and y direction
N, M	total number of CV in x and y direction
$\overline{\mathrm{Nu}}$	mean Nusselt number
Nu_y	local Nusselt number
p_d	dynamic pressure
P_k	shear production of k
Pr	Prandtl number
$\dot{q}_v$	heat source per unit volume
Ra	Rayleigh number
Re	Reynolds number
R_t	turbulent Reynolds number
S_ϕ	source term of a general variable
t	time
T	temperature
T_0	reference temperature
u, v	Cartesian velocity components
u_i	velocity in the x_i-direction
u_τ	friction velocity
W, W_1,.....	horizontal distances (see Fig. 1)
x, y	Cartesian coordinates
x_i	Cartesian coordinate in i-direction
x_n	distance or normal direction to the nearest wall

Greek symbols:

β	thermal expansion coefficient
δ_{ij}	Kronecker delta
ε	dissipation rate of k
κ	Von-Karman constant
λ	thermal conductivity
μ	dynamic viscosity
μ_t	turbulent viscosity
ν	kinematic viscosity
ρ	density
σ_k, σ_ε, σ_T	turb. Prandtl number for k, ε and T, respectively
τ_{ij}	shear-stresses
ψ	stream function

Subscripts:

c	cold
h	hot
in	inlet

Superscripts:

′	fluctuating quantity
*	non-dimensional value

0961–5539/95/010013–21$2.00

Received November 1993
Revised April 1994

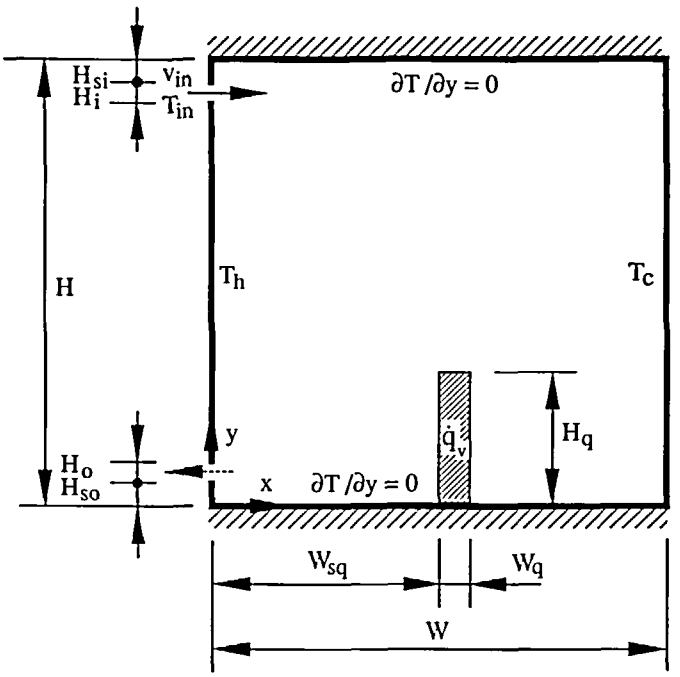

Figure 1 General geometry and boundary conditions

INTRODUCTION

Thermal and fluid-dynamic phenomena involving turbulent natural and mixed convection in enclosures are present in many technological applications such as: ventilation in buildings, liquid storage tanks, active and passive solar systems, electronic circuitry, etc. The optimization of these thermal systems is strongly dependent on the possibilities of their modelization.

Recently, the analysis of natural and mixed convection in enclosures with or without internal solid elements (heat sources, partitions, ...) has attracted the attention of many investigators. For example, Kumar and Yuan[1] study the two-dimensional laminar mixed convection flow in a rectangular enclosure with inlet and outlet ports, for a range of Reynolds and Richardson numbers. Papanicolau and Jaluria[2] analyse the interaction between induced airstreams in enclosures and the buoyancy-driven flow generated by surface heat flux inputs, considering laminar and two-dimensional flow. Studies of the two-dimensional laminar natural convection in partially divided enclosures have been presented, among others, by Kelkar and Patankar[3], Fu *et al.*[4], and Yucel and Acharya[5]. Different papers have been published taking into consideration turbulent flow. Three-dimenisional turbulent natural convection studies have been presented by Rieder and Delfanian[6] and Haghighat *et al.*[7] for partially divided enclosures, and by Davidson[8] for enclosures with internal heat sources. In these studies turbulence is modelled using k-ε turbulence models with wall functions.

The objective of this work is the implementation of numerical techniques (based on segregated algorithms) for simulating natural and mixed turbulent convection. The model problems take into consideration internal obstacles (partitions, heat sources,...) and two-equation k-ε turbulence models are employed.

A generic representation of the geometries analyzed in presented in *Figure 1*, where inflow, outflow and internal heat sources are considered. The first situation analysed, presented as a

reference case, corresponds to enclosures with differentially heated vertical walls and adiabatic top and bottom walls; numerical results have been obtained for two aspect ratios (A=1 and A=30) using several k-ε turbulence models. Preliminary numerical results of two different situations have also been presented; they correspond to a square cavity with differentially heated vertical walls, with inlet and outlet fluid ports in the hotter wall, and to a square cavity with isothermal vertical walls, both at the same temperature, and heated by an internal heat source.

MATHEMATICAL FORMULATION

Governing equations

The time-averaged governing equations of the fluid flow (continuity, momentum and energy) assuming: the Bousinnesq approximation (density variations are relevant only in the buoyancy terms of the momentum equations), fluid Newtonian behaviour, negligible heat friction and influence of pressure on temperature, non-participant radiating medium, may be written in tensor notation as:

$$\frac{\partial u_i}{\partial x_i}=0 \tag{1a}$$

$$\frac{\partial(\rho u_i)}{\partial t}+\frac{\partial(\rho u_j u_i)}{\partial x_j}=-\frac{\partial p_d}{\partial x_i}+\frac{\partial \tau_{ij}}{\partial x_j}-\rho\beta(T-T_0)g_i \qquad (i=1,\ 2) \tag{1b}$$

$$\frac{\partial(\rho T)}{\partial t}+\frac{\partial(\rho u_i T)}{\partial x_i}=-\frac{1}{c_p}\frac{\partial \dot{q}_i}{\partial x_i} \tag{1c}$$

where:

$$\tau_{ij}=\mu\left(\frac{\partial u_i}{\partial x_j}+\frac{\partial u_j}{\partial x_i}\right)-\rho\overline{u_i'u_j'}, \qquad \dot{q}_i=-\lambda\frac{\partial T}{\partial x_i}+c_p\rho\overline{u_i'T'},$$

and, x_i is the Cartesian coordinate in the i-direction ($x_1=x$, $x_2=y$); t the time; u_i the mean velocity in the i-direction ($u_1=u$, $u_2=v$); p_d the mean dynamic pressure; T the mean temperature; g_i the gravitational acceleration in the i-direction ($g_1=0$, $g_2=-g$); T_0 is a reference temperature; and ρ, μ, β, λ, c_p are respectively: the density, the dynamic viscosity, the coefficient of thermal expansion, the thermal conductivity and the specific heat at constant pressure. The turbulent fluctuating velocity in the x_i-direction and the fluctuating temperature are indicated by u_i' and T'.

Due to the small scales of length and time involved in turbulent flows, the direct integration of the Navier-Stokes equations is still not feasible for engineering applications. Thus, turbulence modelling is needed. Among the different turbulence modelling reported in the literature (algebraic models, two-equation models, Reynolds-stress models, large-eddy simulation, etc.), the two-equation k-ε turbulence model stands out because it gives a good balance between accuracy, generality and computational cost.

Eddy-viscosity models, like k-ε turbulence models, use a phenomenological approach in order to evaluate the turbulent stresses and the turbulent heat fluxes. Thus, by analogy with the Stokes viscosity law and the Fourier heat conduction law these terms are written in the form:

$$\rho\overline{u_i'u_j'}=-\mu_t\left(\frac{\partial u_i}{\partial x_j}+\frac{\partial u_j}{\partial x_i}\right)+\frac{2}{3}\rho k\delta_{ij} \tag{2a}$$

$$\rho\overline{u_i'T'}=-\frac{\mu_t}{\sigma_T}\frac{\partial T}{\partial x_i} \tag{2b}$$

where: μ_t and σ_T are the turbulent viscosity and the turbulent Prandtl number, and δ_{ij} is the Kronecker delta. The turbulent Prandtl number is usually taken as a constant (a value of 0.9 has been considered in this work). The turbulent viscosity is related to the turbulent kinetic

energy (k) and the dissipitation of turbulent kinetic energy (ε) by means of the empirical expression of Kolmorogov-Prandtl.

The turbulent kinetic energy and the dissipation of turbulent kinetic energy are obtained from their transport equations. Although the exact form of these equations results from the Navier-Stokes equations, empirical approximations of some terms are necessary. The resulting k-ε equations, together with the Kolmogorov-Prandtl expression, can be written, after taking low-Reynolds-number effects into account, as:

$$\mu_t = c_\mu f_\mu \frac{\rho k^2}{\tilde{\varepsilon}} \tag{3a}$$

$$\frac{\partial(\rho k)}{\partial t} + \frac{\partial(\rho u_i k)}{\partial x_i} = \frac{\partial}{\partial x_i}\left[\left(\mu + \frac{\mu_t}{\sigma_k}\right)\frac{\partial k}{\partial x_i}\right] + P_k + G_k - (\rho\tilde{\varepsilon} + D) \tag{3b}$$

$$\frac{\partial(\rho\tilde{\varepsilon})}{\partial t} + \frac{\partial(\rho u_i \tilde{\varepsilon})}{\partial x_i} = \frac{\partial}{\partial x_i}\left[\left(\mu + \frac{\mu_t}{\sigma_\varepsilon}\right)\frac{\partial \tilde{\varepsilon}}{\partial x_i}\right] + c_{\varepsilon 1}[f_1 P_k + c_{\varepsilon 3} G_k]\frac{\tilde{\varepsilon}}{k} + E - c_{\varepsilon 2} f_2 \frac{\rho\tilde{\varepsilon}^2}{k} \tag{3c}$$

where the variable $\tilde{\varepsilon}$, defined as $\tilde{\varepsilon} = \varepsilon - D/\rho$, is introduced in some turbulence models for computational convenience in order to obtain a zero value of $\tilde{\varepsilon}$ at the wall. The shear production and buoyancy production/destruction of turbulent kinetic energy are respectively: $P_k = -\rho\overline{u_i' u_j'}\,\partial u_i/\partial x_j$ and $G_k = -\beta\rho\overline{u_i' T'}\, g_i$. In these terms the turbulent stresses and heat fluxes are usually evaluated using the standard eddy-diffusivity model (an exception is the Ince and Launder turbulence model).

Turbulence models: empirical values and wall boundary conditions

The turbulence models tested can be divided into two categories: i) Standard k-ε turbulence model using wall functions; ii) Low-Reynolds-Number k-ε turbulence models. Only some of their characteristics are given below (for more details see the references):

i) *Standard* k-ε *turbulence model* using wall functions (SWF). The following empirical values and wall boundary conditions are normally used for natural convection problems[9,10]:

$c_\mu = 0.09$, $c_{\varepsilon 1} = 1.44$, $c_{\varepsilon 2} = 1.92$, $c_{\varepsilon 3} = tanh|u/v|$, $\sigma_k = 1.0$, $\sigma_\varepsilon = 1.3$, $\sigma_T = 0.9$

$f_\mu = f_1 = f_2 = 1$, $D = E = 0$

$k = 0$ at the wall, $\varepsilon = \tilde{\varepsilon} = c_\mu^{3/4} k^{3/2}/(\kappa x_n)$ at the first inner grid point from the wall.

Usually, the ε boundary condition is applied at the nearest grid point from the wall independently of its distance (or x^+ value). Henkes and Hoogendoorn[10] suggest the use of the Dirichlet boundary condition $\varepsilon = \infty$ (or a high value) at the wall instead of the condition indicated above. The standard k-ε model with this ε condition ($\varepsilon = \infty$ at the wall) will be referred to as ST.

ii) *Low-Reynolds-number* k-ε *turbulence models.* The following models have been employed: Jones and Launder[11] (JL), Launder and Sharma[12] (LS), Hoffman[13] (HO), Reynolds[14] (RE), Hassid and Poreh[15] (HP), Lam and Bremhorst[16] (LB), Dutoya and Michard[17] (DM), Chien[18] (CH), To and Humphrey[19] (TH), Nagano and Hishida[20] (NH), Ince and Launder[21] (IL), Davidson[22] (DA), Nagano and Tagawa[23] (NT), and Fan, Lakshminarayana and Barnett[24] (FLB). They will be referred to by the acronym given in brackets. Differences between them arise in the empirical functions (f_μ, f_1, f_2), the extra terms (D, E) and the empirical constants (although many of them employ the same values indicated for the standard k-$-\varepsilon$ model). All of these turbulence models specify k-$=0$ at the wall as a boundary condition; the the ε-equation most of them specify $\tilde{\varepsilon} = 0$ at the wall except: a) $\varepsilon = \nu(\partial^2 k/\partial x_n^2)$ for RE, LB and NT; b) $\partial\varepsilon/\partial x_n = 0$ for DA and FLB; c) $\varepsilon = 2\nu(\partial\sqrt{k}/\partial x_n)$ for TH.

The complete mathematical formulation of these models will only be presented for the IL model. This model uses the same empirical functions, extra terms and boundary conditions as

the LS model, however it introduces two new features: 1) the turbulent heat fluxes in the G_k term are evaluated by means of the generalized gradient diffusion hypothesis (GGDH), that is $\rho\overline{u_i'T'} = -c_0(k/\varepsilon)\rho\overline{u_i'u_k'}\,\partial T/\partial x_k$; 2) in the ε-equation the YAP correction is introduced as an extra source term. Thus:

$$f_\mu = \exp[-3.4/(1+R_t/50)^2],\ f_1 = 1,\ f_2 = 1-0.3\exp(-R_t^2)$$

$$E = 2\nu\mu_t\left(\frac{\partial^2 u_i}{\partial x_j \partial x_k}\right)^2 + 0.83\rho\left(\frac{k^{3/2}}{\tilde{\varepsilon}c_1 x_n} - 1\right)\left(\frac{k^{3/2}}{\tilde{\varepsilon}c_1 x_n}\right)^2\frac{\tilde{\varepsilon}^2}{k}$$

$$D = 2\mu(\partial k^{1/2}/\partial x_j)^2,\ c_1 = 2.5,\ c_0 = (3/2)(c_\mu f_\mu/\sigma_T)$$

where the x_n value has been evaluated as the distance to the nearest wall; R_t is the turbulent Reynolds number defined as $k^2/\nu\tilde{\varepsilon}$.

Boundary conditions

Due to the elliptic nature of the governing equations with respect to the spatial coordinates, boundary conditions have to be specified at all the external boundaries (see *Figure 1*) in order to consider the interactions with the surroundings. At the *solid walls* the fluid velocities are zero; temperatures are specified at the vertical walls ($T = T_h$ for $x = 0$ and $T = T_c$ for $x = W$, with $T_c \leqslant T_h$); adiabatic conditions are given at the top and bottom walls ($\partial T/\partial y = 0$ for $y = 0$ and $y = H$). When internal solids are presented the volumetric heat source, $\dot{q}_t$, is specified. *Inflow conditions* are given specifying the value of the different dependent variables (v_{in}, T_{in}, p_{in}, k_{in}, ε_{in}) at the inlet port. *Outflow conditions* are evaluated specifying zero normal gradients (i.e., $\partial\phi/\partial x = 0$ for $\phi = v$, T, k, ε), except for the horizontal velocity component which is specified from a mass balance.

NUMERICAL PROCEDURE

A structured grid of $N \times M$ control volumes (CV) for the scalar variables (p, T, k, ε) has been used and a staggered grid in the x and y directions has been employed to compute the u and v variables respectively. Due to the presence of internal solid obstacles and/or inlet and outlet ports, the domain is divided into zones where the CV-lines are concentrated symmetrically or partially over its right or left side. For a generic zone r of length L_r, located at a distance x_r from the origin of coordinates, the lines corresponding to N_r number of CV are distributed according to the following expression:

$$xvc(i) = \delta + \frac{\Delta\delta}{2}\left[1 + \tanh\left(2k_{x(r)}\frac{\tilde{i}-1}{n} - k_{x(r)}\right)/\tanh(k_{x(r)})\right], \qquad i = i_r, i_r+1, \ldots, i_r+N_r \qquad (4)$$

where $xvc(i)$ is the cartesian coordinate of the i^{th} CV line in the x-direction; i_r is the first index of the i-CV lines in this zone r; $k_{x(r)}$ is the grid concentration factor in the x-direction in this zone; the other parameters depend on the kind of concentration. For *symmetrical concentration*: $n = N_r$, $\delta = x_r$, $\Delta\delta = L_r$, $\tilde{i} = i - i_r + 1$; for *concentration to the right side*: $n = 2N_r$, $\delta = x_r$, $\Delta\delta = 2L_r$, $\tilde{i} = i - i_r + 1$; for *concentration to the left side*: $n = 2N_r$, $\delta = x_r - L_r$, $\Delta\delta = 2L_r$, $\tilde{i} = i + N_r - i_r + 1$. An analogous procedure for the CV lines in the y-direction is used.

Shear-stresses and heat fluxes are evaluated and stored in the points indicated in *Figure 2*, where the CV for the scalar quantities are defined by the discontinuous lines, and the main nodes are indicated by the standard notation (i.e., P, W, E, S, N). Their implementation in the discretized momentum and energy equations is done by means of the flux-stress formulation by Raithby *et al.*[25]. Convective terms are discretized using the first-order numerical scheme EDS[25] and, occasionally, the second-order numerical scheme QUICK[26]; due to numerical stability problems, the latter scheme has not been applied to the k and ε equations.

The coupling between the governing equations is made by means of the SIMPLEX algorithm

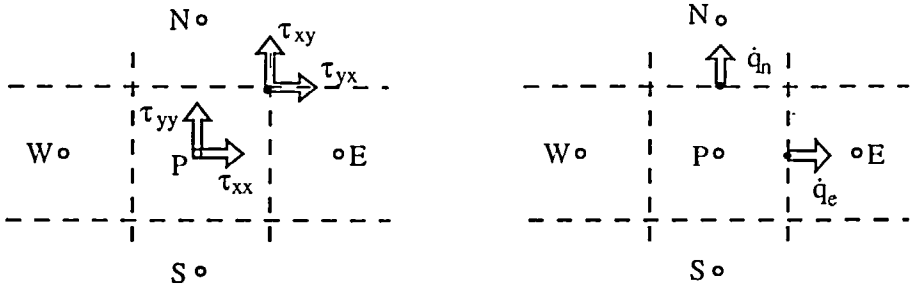

Figure 2 Storage location for shear-stresses (τ_{ij}) and heat fluxes ($\dot{q}_j$)

proposed by Van Doormaal and Raithby[27]. The momentum, pressure correction, temperature, turbulent kinetic energy and dissipation rate of turbulent kinetic energy equations are solved sequentially using the modified strongly implicit procedure (MSIP) of Schneider and Zedan[28]. When there are internal solids in the enclosure, a zero value of velocity and turbulent viscosity is assigned to these zones. The energy equation is solved in the whole domain with a special treatment at the interfaces (especially important when radiation between surfaces is considered[29]).

In the k and ε equations the source terms are linearized in the usual form[25], that is: $S_\phi = S_C + S_P \phi_P$, where S_ϕ is the source term associated with the dependent variable ϕ. In order to prevent numerical instabilities and avoid negative values for the k and ε variables, all the production terms have been included in the S_C term (giving a positive S_C value) and all the dissipation terms in the S_P term (giving a negative S_P value). Thus, for example, in the k-equation the source terms are evaluated in the form: $S_C = P_k + \max(G_k, 0)$, and $S_P = -[\rho\tilde{\varepsilon} + D - \min(G_k, 0)]/k$.

When only a steady-state solution is desired, under-relaxation is introduced by means of a pseudo-transient scheme based on the E-factor formulation[25,27]. The E-factor acts as a parameter for allowing and/or improving the rate of convergence. Global convergence is achieved when the mass balance is verified in all control volumes within a prescribed value (typically 10^{-9}) and when the residual values of the different equations are sufficiently low (typically 10^{-10}). A control of the evolution of different values (mean Nusselt numbers, maximum velocities, stream function at given points, etc) is also done in order to assure good convergent solutions.

NUMERICAL RESULTS

Based on the geometry presented in *Figure 1*, the air flow (Pr = 0.71) for three different cases has been studied:

- *Case 1:* a cavity with differentially heated vertical walls taking two aspect ratios of 1 and 30 into consideration.
- *Case 2:* a square cavity with differentially heated vertical walls and with inlet and outlet fluid ports in the hotter wall; two inlet velocities are considered.
- *Case 3:* a square cavity with isothermal vertical walls, both at the same temperature, and heated with a solid element located on the floor at the middle of the horizontal plane; two volumetric heat sources are considered.

For all the cases, adiabatic top and bottom walls are considered. *Table 1* shows the values of the geometry and boundary conditions selected.

Numerical results are presented in the following non-dimensional form: $x^* = x/L_{ref}$, $y^* = y/L_{ref}$, $u^* = u/(g\beta\Delta T_{ref} L_{ref})^{1/2}$, $v^* = v/(g\beta\Delta T_{ref} L_{ref})^{1/2}$, $T^* = (T - T_c)/\Delta T_{ref}$, $\mu_t^* = \mu_t/\mu$. As a reference length (L_{ref}), the height H of the cavity has been chosen for all the cases; the reference temperature (ΔT_{ref}) is defined as $T_h - T_c$ for the first and second cases, and as $(\dot{q}_t H_q W_q / 4\lambda)^{1/2}$ for the third case. The characteristic non-dimensional numbers are: $\mathrm{Pr} = \mu c_p/\lambda$, $\mathrm{Ra} = g\beta\Delta T_{ref} L_{ref}^3 \mathrm{Pr}/\nu^2$, $\mathrm{Re} = 2H_t v_{in}/\nu$, $Nu_y = -(L_{ref}/\Delta T_{ref})(\partial T/\partial x)_{(x=0 \text{ or } x=W,\, y)}$.

Table 1 Geometry and boundary conditions (see *Figure 1*) of the different cases studied

	Case 1		Case 2		Case 3	
	(a)	(b)	(a)	(b)	(a)	(b)
H (m)	2.07	1.8628	2.07	2.07	2.07	2.07
W (m)	2.07	0.0621	2.07	2.07	2.07	2.07
A = H/W	1	30	1	1	1	1
$H_i = H_o$ (m)	0	0	0.10	0.10	0	0
$H_{si} = H_{so}$ (m)	–	–	0.10	0.10	–	–
H_q (m)	0	0	0	0	0.50	0.50
W_q (m)	–	–	–	–	0.11	0.11
W_{sq} (m)	–	–	–	–	0.98	0.98
T_h (C)	27	50	27	27	15	15
T_c (C)	15	10	15	15	15	15
v_{in} (m/s)	–	–	0.10	0.25	–	–
T_{in} (C)	–	–	27	27	–	–
$\dot{q}_v$ (W/m².m)	–	–	–	–	1125	2250

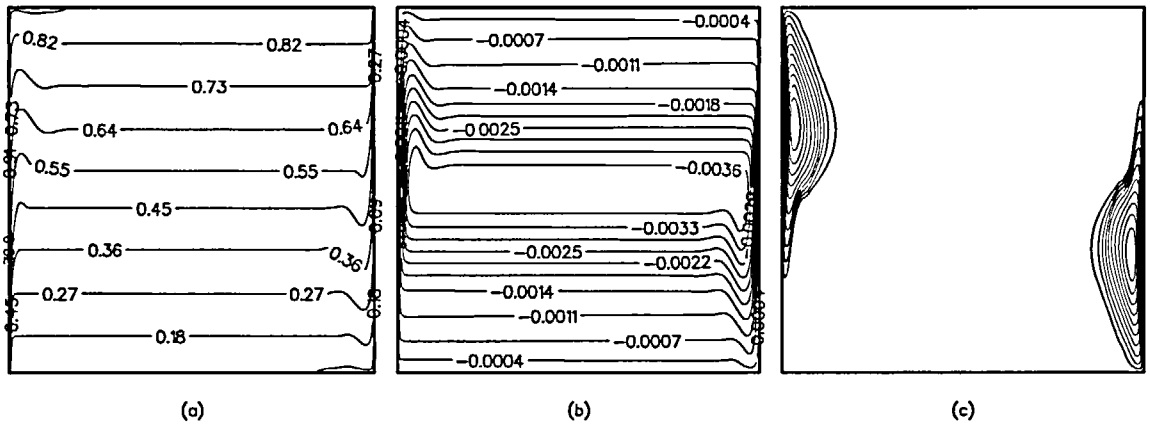

Figure 3 *Case 1a* Computed isotherms (a), streamlines (b), and iso-turbulent viscosity lines (c) using the ST model; 99 × 99 grid

Case 1a

This case corresponds to a square cavity with differentially heated vertical walls ($Ra = 10^{10}$) and adiabatic top and bottom walls. The isotherms, streamlines, and iso-turbulent viscosity lines, using the ST turbulence model and a grid of 99 × 99 CV, are shown in *Figure 3*. It can be observed that the movement of the flow is concentrated in the vicinity of the vertical walls creating a boundary layer. In the initial zones (lower part of the hot wall and upper part of the cold wall) the boundary layer is laminar and at some distance it becomes turbulent. The greatest temperature gradients appear in the vertical thermal boundary layers while the core remains thermally stratified. For this case (and *Case 1b*), numerical calculations give symmetric solutions with respect to the centre of the cavity.

The influence of the grid concentration factors is shown in *Table 2* using the ST model and a grid of 63 × 63 CV. The grid concentration factor k_x has little influence on the results because, for the selected range, enough number of grid points are located between the wall and the maximum vertical velocity (from 5 to 14 at $y^* = 0.5$); the influence of the k_y factor is more

Table 2 *Case 1a* Influence of the grid concentration factors, ST model, 63 × 63 grid

			k_x		
			3.0	4.0	5.0
		(a)	134.1	135.9	136.7
	2.0	(b)	0.18568	0.18524	0.18528
		(c)	18.8	19.2	19.6
		(a)	138.7	140.6	141.0
k_y	3.0	(b)	0.18572	0.18554	0.18581
		(c)	21.6	21.9	22.3
		(a)	–	142.9	143.3
	4.0	(b)	–	0.18661	0.18656
		(c)	–	23.2	23.7

(a) $\overline{Nu}$; (b) v^* max (at $y=H/2$); (c) μ_t^* max.

Table 3 *Case 1a* Influence of grid refinement using the ST model

Grid	$\overline{Nu}$ at $x^*=0$	Nu_y max at $x^*=0$	u^* max at $x^*=0.5$	v^* max at $y^*=0.5$	$\partial T^*/\partial y^*$ at centre	μ_t^* max
45 × 45	142.8	414.1	0.0144	0.1872	0.659	34.1
63 × 63	140.6	422.3	0.0145	0.1855	0.714	32.0
81 × 81	137.2	428.8	0.0145	0.1850	0.785	28.9
99 × 99	132.8	434.2	0.0143	0.1858	0.892	27.5
135 × 135	124.9	440.2	0.0142	0.1924	1.202	22.8
171 × 171	120.6	442.5	0.0141	0.2029	1.513	20.0

important as can be observed in the heat transfer and turbulent viscosity predictions. The results presented here have been obtained using grid concentration factors of 4 and 3 in the x and y directions respectively.

The influence of grid refinement (from 45 × 45 to 171 × 171 CV) using the ST model is shown in *Table 3*. Grid refinement strongly affects the location of the transition point in the vertical boundary layers as can be seen in the local Nusselt number distribution in *Figure 4*. In the lower part of the wall the boundary layer is laminar and a reduction of heat transfer is produced due to the increase of the boundary layer thickness in the flow direction; at a certain distance an abrupt increase in the heat transfer rate indicates that the flow becomes turbulent. When the grid is refined the transition point moves upstream giving: lower levels of turbulence, lower heat transfer rates, and higher values of the stratification at the centre. Compared with the empirical correlation $Nu=0.046Ra^{1/3}$ (verified by Paolucci[30] using a two-dimensional direct numerical simulation for a square cavity at $Ra=10^{10}$), a mean Nusselt number overprediction of more than 22% is produced with the ST model; however more refined grids have to be tested in order to obtain a grid independent solution. Similar trends were obtained by the authors[31] for a $Ra=5\cdot10^{10}$ using grids up to 189 × 189 CV; no important differences were obtained with the QUICK scheme. A comparison of the numerical solution obtained using the ST model and different density grids is also presented in *Figure 4*, where the mean Nusselt number and the velocity, temperature and turbulent viscosity distributions at different sections are shown.

Table 4 summarizes the results obtained with other turbulence models using two grids of 45 × 45 and 81 × 81 CV. In comparison with the ST model, the SWF model gives slightly higher heat transfer rates and turbulence levels. The IL, LS and HO models predict a laminar solution, while the CH, NH and DM models reduce significantly turbulence levels when the grid is refined.

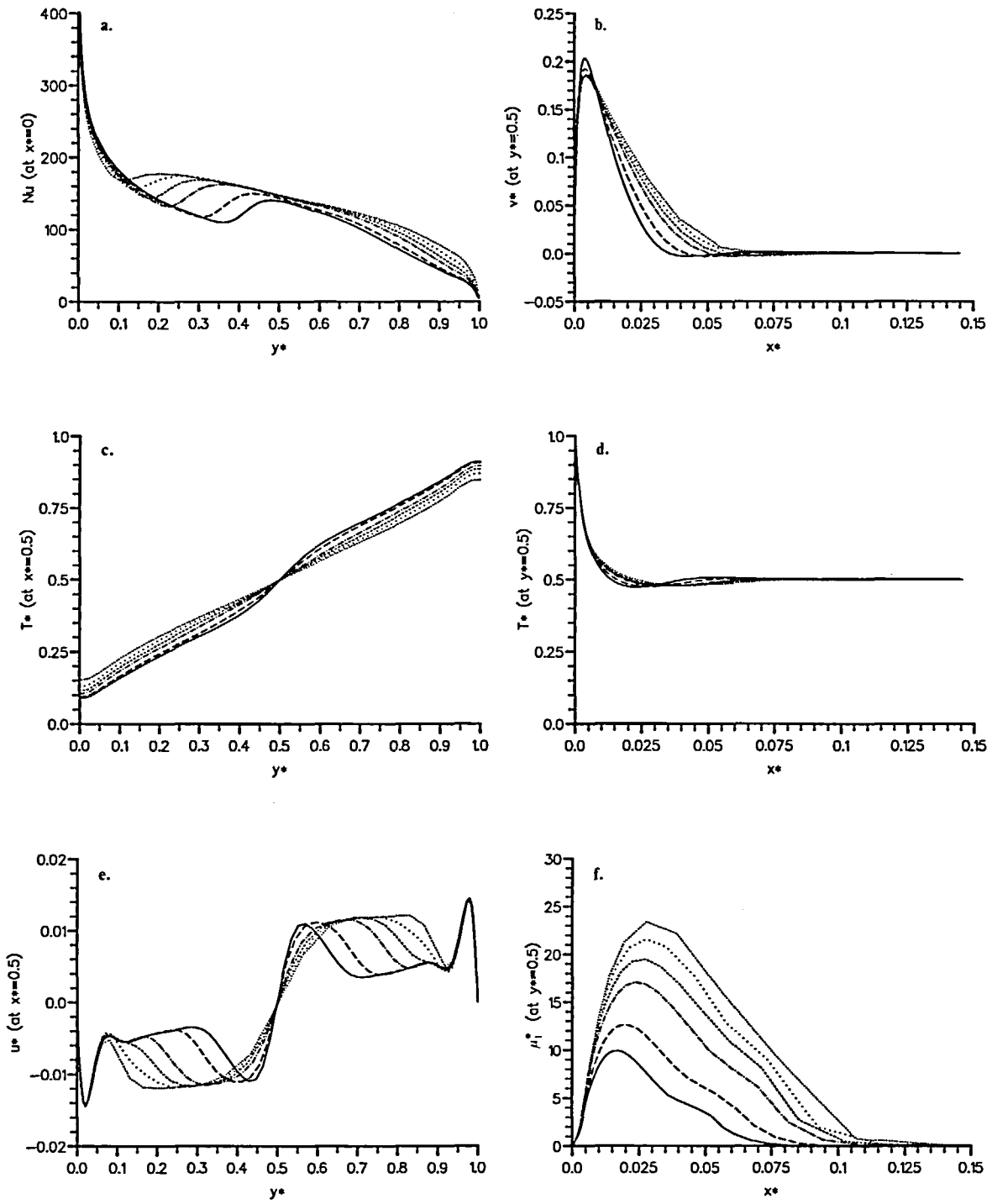

Figure 4 *Case 1a* Local Nusselt number at $x^*=0$ (a), and non-dimensional vertical velocity at $y^*=0.5$ (b), temperature at $x^*=0.5$ (c) and at $y^*=0.5$ (d), horizontal velocity at $x^*=0.5$ (e) and turbulent viscosity at $y^*=0.5$ (f), using the ST model and different density grids (·····: 45 × 45; • • • • •: 63 × 63; - - - -: 81 × 81; ·–·–: 99 × 99; – – –: 135 × 135; ——: 171 × 171)

Table 4 *Case 1a* Influence of grid refinement on different turbulence models

Turb. model	Grid $N \times M$	$\overline{Nu}$ at $x^*=0$	Nu_y max at $x^*=0$	u^* max at $x^*=0.5$	v^* max at $y^*=0.5$	$\partial T^*/\partial y^*$ at centre	μ_t^* max
SWF	45×45	148.5	421.4	0.0149	0.1874	0.679	33.2
	81×81	144.9	434.3	0.0147	0.1841	0.763	30.2
CH	45×45	101.4	425.6	0.0152	0.2312	0.877	17.0
	81×81	97.8	427.4	0.0147	0.2691	1.047	7.5
NH	45×45	100.0	422.2	0.0148	0.2308	0.896	22.2
	81×81	97.1	427.5	0.0155	0.2667	0.985	5.3
DM	45×45	96.1	422.3	0.0159	0.2633	0.954	5.3
IL, LS, HO	45×45	95.8	421.2	0.0221	0.2633	0.957	0

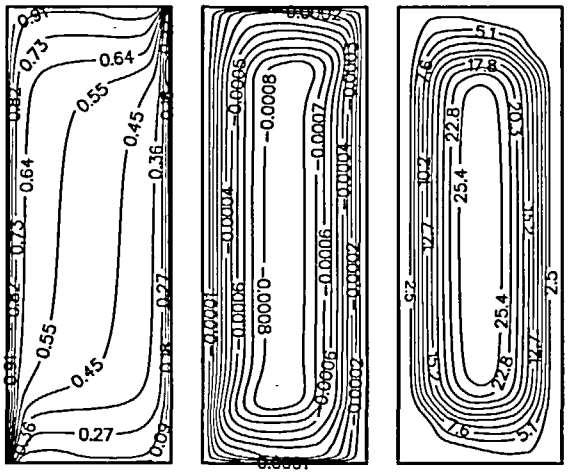

Figure 5 *Case 1b* Computed isotherms (a), streamlines (b), and iso-turbulent viscosity lines (c) using the IL model; 81×81 grid

Case 1b

This case corresponds to a differentially heated tall cavity with an aspect ratio of 30 and a Rayleigh number (based on height) of $2.43 \cdot 10^{10}$. Isotherms, streamlines, and iso-turbulent viscosity lines, using the IL turbulence model and a grid of 81×81 CV, are shown in *Figure 5*. This case presents a significantly fully developed one-dimensional flow in most of the domain, except in the lower and upper zones. In the core region the stratification is nearly zero and the highest levels of turbulence are produced in the vertical midplane.

The influence of the grid concentration factor, in both x and y directions, using the IL model and a grid of 45×45 CV, has been tested. Variations of the k_x concentration factor in the range from 2.0 to 4.0 have little influence on the numerical results because, for the selected range, enough grid nodes are located between the wall and the point of maximum vertical velocity (between 8 to 14 grid nodes in the fully developed zone); variations from 1 to 3 in the k_y concentration factor have also little influence due to the one-dimensional flow structure in most

Table 5 *Case 1b* Influence of grid refinement using different turbulence models

Turb. model	Grid $N \times M$	$\overline{Nu}$ at $x=0$	Nu_y max at $x=0$	u^* max at $x=W/2$	v^* max at $y=H/2$	ψ^* at centre	μ_t^* max
	45×45	283.1	545.4	0.0323	0.07843	−0.000775	33.6
ST	63×63	283.9	546.3	0.0315	0.07801	−0.000774	33.6
	81×81	284.1	539.1	0.0314	0 07782	−0.000774	33.6
	45×45	166.0	570.1	0.0388	0.09836	−0.000843	28.9
IL	63×63	164.4	582.8	0.0398	0.09844	−0.000848	28.0
	81×81	163.3	581.7	0.0411	0.09833	−0.000850	27.9
	45×45	174.4	576.4	0.0345	0.07013	−0.000484	52.5
FLB	63×63	172.6	578.3	0.0355	0.07202	−0.000492	51.8
	81×81	170.0	577.1	0.0374	0.07415	−0.000506	50.5

Table 6 *Case 1b* Results obtained using the QUICK scheme and two turbulence models

Turb. model	Grid $N \times M$	$\overline{Nu}$ at $x=0$	Nu_y max at $x=0$	u^* max at $x=W/2$	v^* max at $y=H/2$	ψ^* at centre	μ_t^* max
IL	45×45	165.4	599.9	0.0410	0.09861	−0.000847	28.3
FLB	45×45	174.5	593.7	0.0375	0.07010	−0.000484	52.6

of the cavity. All the cases presented here have been obtained using concentration factors of 4 and 3 in the x and y directions respectively.

The influence of the grid refinement using three turbulence models (ST, IL and FLB) is shown in *Table 5*. For the ST and IL models small differences are produced when the grid is refined from 45×45 CV to 81×81 CV (similar numerical results using these turbulence models were also reported by Henkes and Hoogendoorn[32]). The FLB model gives higher differences specially in the velocity values. For the same number of grid points, the second-order scheme QUICK, see *Table 6*, gives slightly more accurate results than the first order scheme EDS.

A comparison of different k-ε turbulence models and the experimental results reported by Dafa'Alla and Betts[33] for a fully developed one-dimensional Boussinesq flow in an infinitely tall air cavity is presented in *Table 7*. The heat transfer rate (mean Nusselt number) is overpredicted for all of the turbulence models tested (specially for the high Reynolds-number models SWF and ST); the best agreement is obtained for the IL and LB models. The maximum vertical velocity is generally underpredicted; the SWF and ST give similar (or even better) results than some of the low-Reynolds-number turbulence models tested; the best agreement is obtained with the CH, IL and DM models. The maximum turbulent viscosity is well predicted for most of these models except for LB, RE, NH, NT and FLB. In conclusion, for this case and for the experimental values tested, the most accurate prediction has been obtained with the IL model.

A comparison between ST and the IL model is also presented in *Figure 6* for the mean Nusselt number and the non-dimensional velocity, temperature, and turbulent viscosiy at the cavity mid height.

Case 2

The second case presented corresponds to a square cavity with differentially heated vertical walls ($Ra = 10^{10}$), adiabatic top and bottom walls, and with inlet and outlet fluid ports at the hotter wall. The isotherms, streamlines and iso-turbulent viscosity lines, for two inlet velocities of 0.10 m/s ($Re = 1275$) and 0.25 m/s ($Re = 3187$), are presented in *Figure 7* (using the SWF model and a grid of 90×90 number of CV). In comparison with *Case 1a*, and even for the lower inlet

Table 7 *Case 1b* Numerical results obtained with different turbulence models for a grid of 45 × 45. The difference (in percentage) respect to the experimental data by Daffa'Alla and Betts[33] ($\overline{Nu}$ = 149; ι^* max (at $y = H/2$) = 0 09567; μ_t^* max at the centre = 30.4) are indicated in brackets

Turb. model	$\overline{Nu}$	ι^* max at $y = H/2$	μ_t^* at centre
ST	283.1 (90%)	0.07843 (−18%)	33.6 (11%)
SWF	346.9 (133%)	0.07537 (−21%)	34 8 (14%)
JL	196.1 (32%)	0.08416 (−12%)	29.6 (−3%)
LS	213.3 (43%)	0.07532 (−21%)	32.7 (8%)
HO	190.9 (28%)	0.11516 (20%)	21.5 (−29%)
RE	195.5 (31%)	0 06456 (−33%)	43.1 (42%)
HP	231.4 (55%)	0.08232 (−14%)	32.5 (7%)
LB	167.0 (12%)	0.07438 (−22%)	50.0 (64%)
DM	193.9 (30%)	0.08619 (−10%)	33.5 (10%)
CH	180.5 (21%)	0.09421 (−2%)	37.2 (22%)
TH	203.0 (36%)	0.07610 (−20%)	31.7 (4%)
NH	183.3 (23%)	0.06871 (−28%)	49.0 (61%)
IL	166.0 (11%)	0.09836 (3%)	28.9 (−5%)
DA	261.0 (45%)	0.07323 (−23%)	34.6 (14%)
NT	183.3 (23%)	0 07063 (−26%)	51.9 (71%)
FLB	174.4 (17%)	0.07415 (−22%)	52.5 (73%)

Table 8 *Case 2a* Influence of grid refinement using different turbulence models

Turb. model	SWF		ST	IL	
$N \times M$	45 × 45	90 × 90	45 × 45	45 × 45	90 × 90
u^* max[(a)]	0.05549	0.07272	0.05727	0.06753	0.06269
$\lvert\iota^*\rvert$max[(b)]	0.24760	0.24470	0.24511	0.39463	0.39622
T^* [(c)]	0.7838	0.7759	0.7872	0.9988	1.0010
ψ^*[(c)]	−0.00718	−0.00722	−0.00717	−0.00753	−0.00629
$\partial T^*/\partial y^*$[(c)]	0.684	0.697	0.653	0.0014	0.0025
$\overline{Nu}$[(d)]	53.1	52.5	50.1	7.8	6.0
$\overline{Nu}$[(e)]	275.8	279.9	265.9	161.4	161.9
μ_t^* max	57.9	55.6	58.7	20.4	0

(a) at $x^* = 0.5$; (b) at $y^* = 0.5$; (c) at the centre ($x^* = y^* = 0.5$); (d) at $x^* = 0$; (e) at $x^* = 1$

velocity, the flow structure is greatly affected by the inlet and outlet ports. A recirculation zone appears just below the upper main stream; the flow tends to move near the walls without affecting the core, where a weak recirculating zone is observed for the case with lower inlet velocity. In both situations, the upper part of the cavity remains nearly isothermal (due to the hot wall jet) while the rest of the core remains thermally stratified; when the inlet velocity increases the isothermal region increases. The flow structure enhances the heat transfer at the cold wall ($x^* = 1$) while it is considerably reduced at the hot wall ($x^* = 0$). The greatest levels of turbulence are located in the upper and lower right part of the cavity.

The inflow turbulent kinetic energy has been estimated assuming a given percentage value of the mean kinetic energy at the inlet ($k_{in} = \alpha_k u_{in}^2$ where $\alpha_k = 0.006$), while its dissipation rate is estimated from the expression $\varepsilon_{in} = c_\mu^{0.75} k_{in}^{1.5} / \alpha_\varepsilon H_{in}$ where $\alpha_\varepsilon = 0.015$. Two density grids of 45 × 45 and 90 × 90 number of CV have been used, together with grid concentration factors of 4 and 3 in the x and y directions respectively.

In *Table 8* some numerical results obtained for the lower inlet velocity, using different turbulence models and two density grids, are presented. The SWF model produces small

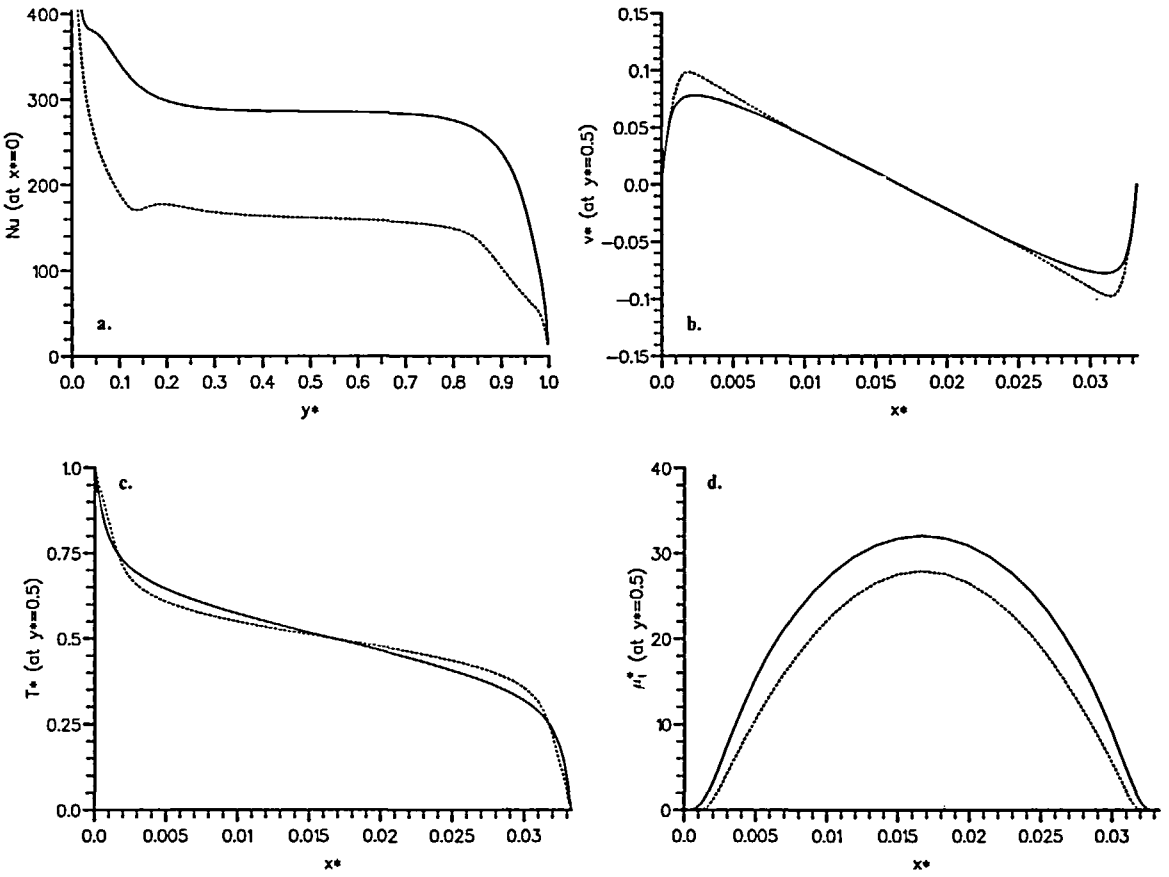

Figure 6 *Case 1b* Local Nusselt numbers at $x^*=0$ (a) and non-dimensional vertical velocity (b), temperature (c) and turbulent viscosity (d) distributions at $y^*=0.5$, using two turbulence models (solid line: ST, dashed line: IL)

differences when the grid is refined (less than 5%, except for the horizontal velocity component). The ST model gives similar results to the SWF model. For the IL model (and also for the LS model), damping effects collapse turbulence giving a laminar solution when the grid is refined.

For the higher inlet velocity (*Case 2b*), some numerical results using different turbulence models and two density grids are presented in *Table 9*. When the grid is refined the main differences are produced for the horizontal velocity component and for the stratification at the centre. For this case, similar results have also been obtained with the ST and the SWF models. In comparison with the SWF model, the IL model gives significantly lower heat transfer rates and stratification values (due to the higher nearly isothermal zone predicted with this model); differences between the maximum horizontal and vertical velocity components are less than 4% and 14% respectively. A comparison between these turbulence models is also presented in *Figure 8* which shows the Nusselt number distribution at the vertical walls and the non-dimensional velocities and temperatures at the cavity mid $x^*=0.5$.

Finally, some results obtained using the second-order numerical scheme QUICK are presented in *Table 10* for the higher inlet velocity case and using both the SWF and the IL models. Taking the results obtained with the EDS scheme using the 90×90 grid as a reference solution, the QUICK scheme gives slightly better predictions than the EDS scheme, particularly for the velocity profiles.

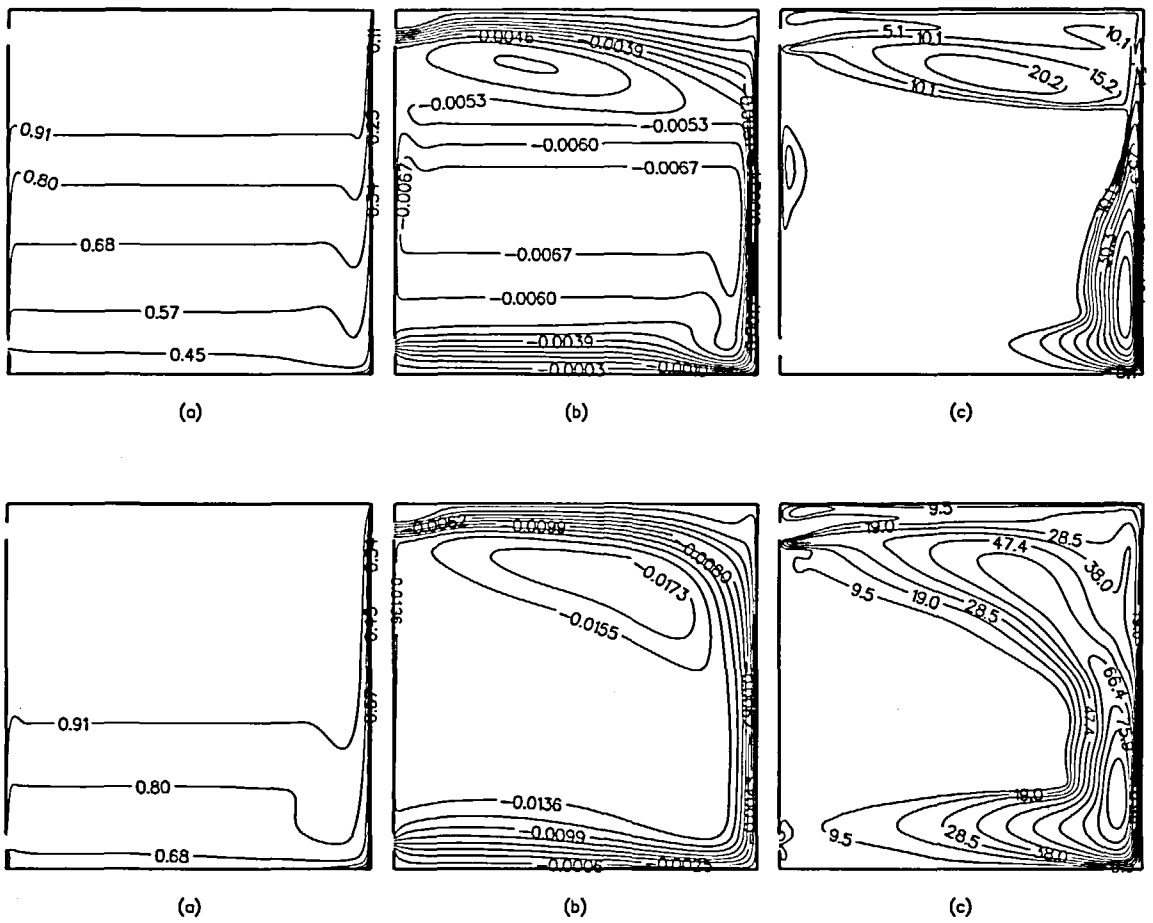

Figure 7 *Case 2* Computed isotherms (a), streamlines (b), and iso-turbulent viscosity lines (c) corresponding to *Case 2a* (upper row) and *Case 2b* (lower row); SWF model, 90 × 90 grid

Table 9 *Case 2b* Influence of grid refinement using different turbulence models

Turb. model	SWF		ST	IL	
$N \times M$	45 × 45	90 × 90	45 × 45	45 × 45	90 × 90
u^* max[a]	0.17853	0.19967	0.17845	0.18333	0.20800
$\|v^*\|$max[b]	0.31751	0.32292	0.31579	0.31571	0.32364
$T^{*(c)}$	0.9523	0.9469	0.9531	0.9735	0.9749
$\psi^{*(c)}$	−0.01369	−0.01383	−0.01366	−0.01406	−0.01375
$\partial T^*/\partial y^{*(c)}$	0.305	0.344	0.290	0.098	0.045
$\overline{Nu}^{(d)}$	31.6	33.7	27.4	13.9	13.5
$\overline{Nu}^{(e)}$	336.4	341.3	319.3	219.5	214.7
μ_t^* max	106.3	104.4	107.4	98.3	94.7

(a) at $x^* = 0.5$; (b) at $y^* = 0.5$; (c) at the centre ($x^* = y^* = 0.5$); (d) at $x^* = 0$; (e) at $x^* = 1$

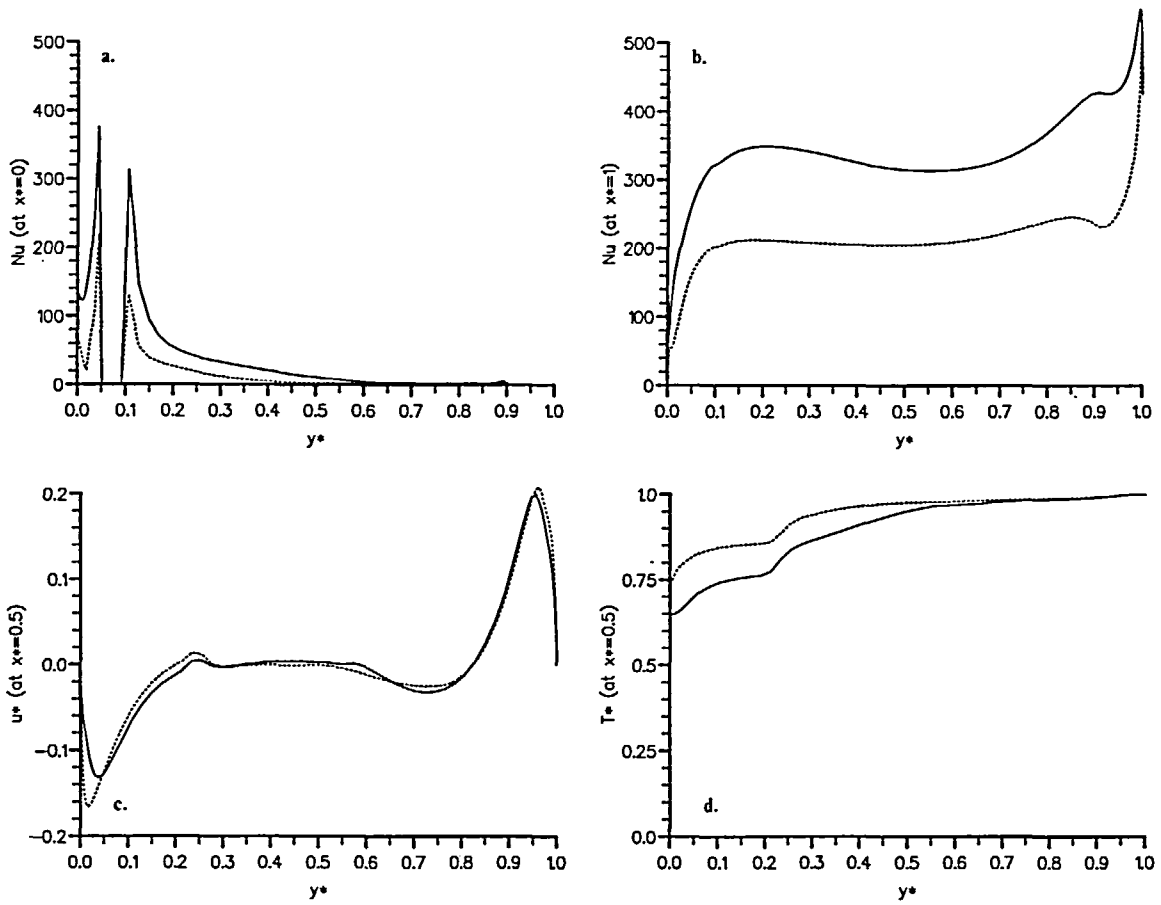

Figure 8 *Case 2b* Local Nusselt number at $x^*=0$ (a) and at $x^*=1$ (b), and non-dimensional horizontal velocity (c) and temperature (d) distribution at $x^*=0.5$, using the SWF model (solid line) and the IL model (dashed line); 90 × 90 grid

Table 10 *Case 2b* Results obtained with the QUICK scheme, 45 × 45 grid

Turbulence model	$\overline{Nu}$ at $x^*=0$	$\overline{Nu}$ at $x^*=1$	u^* max at $x^*=0.5$	$\lvert v^*\rvert$max at $y^*=0.5$	$\partial T^*/\partial y^*$ at centre	μ_t^* max
SWF	*27.8*	*342.2*	*0.18716*	*0.31481*	*0.314*	*113.6*
IL	11.3	220.1	0.19438	0.31575	0.057	110.9

Case 3

The third case presented corresponds to a square cavity with isothermal vertical walls (both at the same temperature), adiabatic top and bottom walls, and heated by a solid element (with internal heat sources) located on the floor at the middle of the horizontal plane. The thermophysical properties of the solid element are: $\rho_s=1700$ Kg/m^3, $\lambda_s=0.5$ W/mK, $c_{ps}=843$ J/Kg. The isotherms, streamlines and iso-turbulent viscosity lines corresponding to two volumetric heat source values ($\dot{q}_v$), 1125 W/m^2.m (Ra $=2.02\cdot10^{10}$, *Case 3a*) and 2250 W/m^2.m (Ra $=2.86\cdot10^{10}$, *Case 3b*), are shown in *Figure 9*, using the SWF model and a grid of 90 × 90 CV. Above the heat

source a turbulent buoyant plume is formed and when it reaches the ceiling it spreads laterally and goes down near the vertical walls, creating a recirculating flow over the entire enclosure. The enclosure is nearly isothermal in the upper part due to the vortex pattern in this region.

Grid lines have been concentrated near the walls using grid concentration factors of 4 and 3 in the x and y directions respectively; two density grids of 45×45 and 90×90 CV have been used. Different turbulence models have been tested using a pseudo-transitory numerical scheme in order to obtain a steady-state solution; the SWF, ST and FLB models give stable convergent solutions, while no stable convergence but an oscillatory behaviour has been obtained with the IL, LS and CH models. Although numerical results exhibit symmetrical solutions in the middle vertical plane, symmetry boundary conditions are not imposed because these symmetries might not be sustained for all the regimes.

For the lower value of the heat source (*Case 3a*), some results have been presented in *Table 11* to illustrate the influence of the grid refinement using the SWF and FLB models; results obtained with IL model have also been presented even though no stable convergent solution has been obtained. When the grid is refined: – the maximum turbulent viscosity increases for the SWF model (about 10%) while it decreases for the FLB model (about 4%); – the rest of the values presented increase (less than 10% except the stratification, which is more than 25%). Maximum temperatures are reached inside the solid element. In comparison with the SWF model: – higher

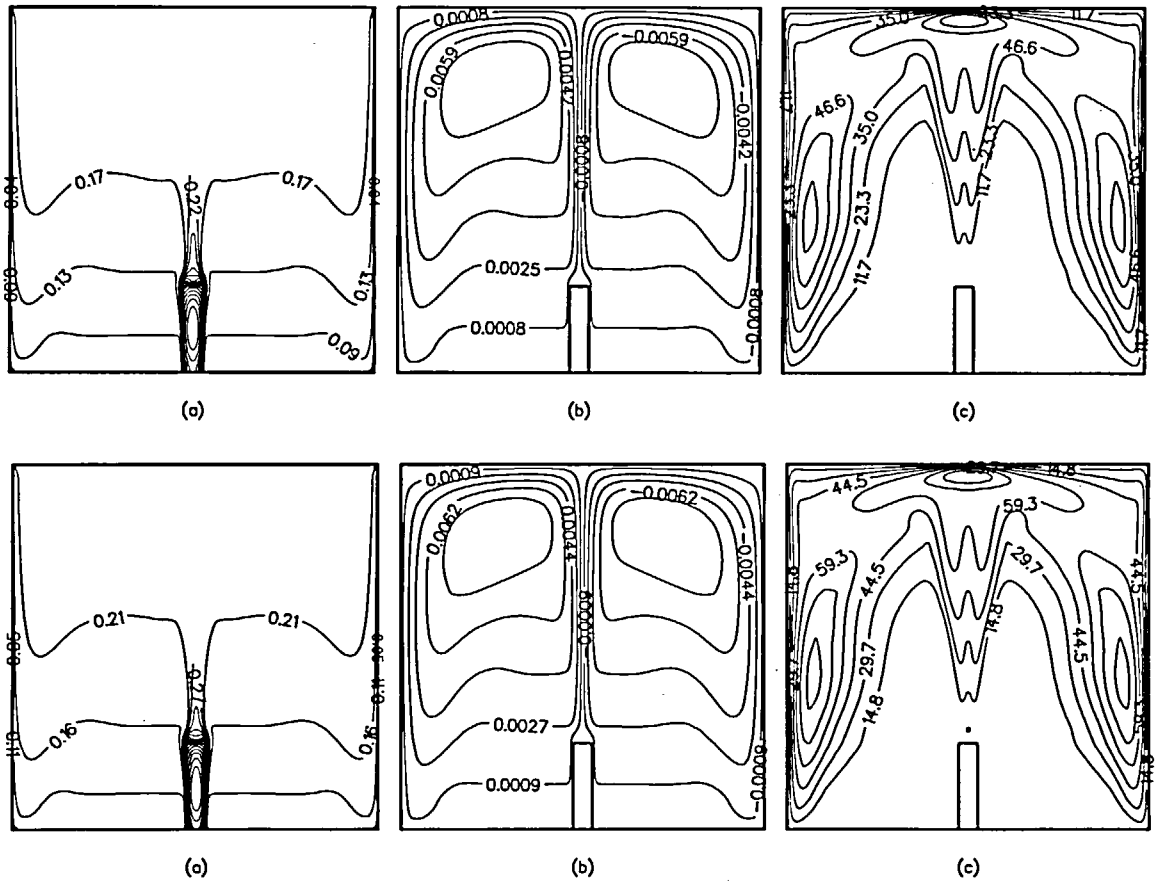

Figure 9 *Case 3* Computed isotherms (a), streamlines (b), and iso-turbulent viscosity lines (c) corresponding to *Case 2a* (upper row) and *Case 2b* (lower row); SWF model, 90×90 grid

Table 11 *Case 3a* Influence of grid refinement using different turbulence models

Turb. model	SWF		FLB		IL
$N \times M$	45×45	90×90	45×45	90×90	45×45
u^* max	0.09825	0.10505	0.11517	0.12756	0.18830
at (x^*, y^*)	(0.652, 0.985)	(0.666, 0.980)	(0.599, 0.993)	(0.608, 0.992)	(0.537, 0.997)
v^* max	0.18942	0.19254	0.22921	0.23260	0.25134
at (x^*, y^*)	(0.471, 0.242)	(0.471, 0.242)	(0.529, 0.242)	(0.528, 0.242)	(0.500, 0.788)
T^* max	0.871	0.911	1.063	1.040	1.045
at (x^*, y^*)	(0.500, 0.130)	(0.504, 0.120)	(0.500, 0.171)	(0.504, 0.160)	(0.500, 0.171)
$\partial T^*/\partial y^{*(a)}$	−0.283	−0.452	−0.331	−0.449	−0.331
$\overline{Nu}^{(b)}$	48.57	48.60	48.58	48.46	48.45
μ_t^* max	73.6	81.6	70.8	68.2	54.5
at (x^*, y^*)	(0.928, 0.383)	(0.496, 0.968)	(0.961, 0.383)	(0.956, 0.430)	(0.072, 0.597)

(a) at the centre $(x^* = y^* = 0.5)$; (b) at $x^* = 1$

Table 12 *Case 3b* Influence of grid refinement using different turbulence models

Turb. model	SWF		FLB		IL
$N \times M$	45×45	90×90	45×45	90×90	45×45
u^* max	0.10466	0.11133	0.11966	0.13270	0.14696
at (x^*, y^*)	(0.652, 0.985)	(0.666, 0.93)	(0.599, 0.993)	(0.608, 0.992)	(0.566, 0.995)
v^* max	0.20388	0.20556	0.24861	0.26734	0.23790
at $(x^*, y^*$	(0.471, 0.242)	(0.472, 0.242)	(0.471, 0.242)	(0.504, 0.541)	(0.500, 0.597)
T^* max	1.068	1.116	1.334	1.304	1.315
at (x^*, y^*)	(0.500, 0.0958)	(0.504, 0.103)	(0.500, 0.171)	(0.504, 0.160)	(0.500, 0.171)
$\partial T^*/\partial y^{*(a)}$	−0.316	−0.505	−0.393	−0.706	−0.359
$\overline{Nu}^{(b)}$	68.68	68.62	68.69	68.62	68.52
μ_t^* max	92.8	103.8	89.8	88.6	71.7
at (x^*, y^*)	(0.928, 0.383)	(0.496, 0.968)	(0.928, 0.448)	(0.956, 0.430)	(0.072, 0.597)

(a) at the centre $(x^* = y^* = 0.5)$; (b) at $x^* = 1$

maximum velocities and temperatures are obtained with the FLB model (less than 18%); – all the models give similar values for the stratification at the centre; – lower turbulence viscosity is obtained for the low-Reynolds-number turbulence models (20% for the FLB model). For this case ST model gives similar results to SWF model. The mean Nusselt depends neither on the turbulence models nor on the number of grid points, because it represents the non-dimensional heat loss to the exterior and it has to be equal to half of the non-dimensional heat generated by the heat source.

Table 12 summarizes the numerical results obtained for the higher value of the heat source tested (*Case 3b*), using the SWF, FLB and IL models and two density grids. These results show similar trends to the ones indicated for the *Case 3a*, except the dicrepancies for the stratification at the centre beween the SWF and FLB models. A comparison between the SWF and FLB models is also presented in *Figure 10* using a grid of 90×90 CV.

CONCLUSIONS

Finite-difference techniques based on control-volume formulation and segregated algorithms have been implemented in order to simulate turbulent natural and mixed convection flow in enclosures. Inflow and outflow ports together with internal solid elements with heat sources can

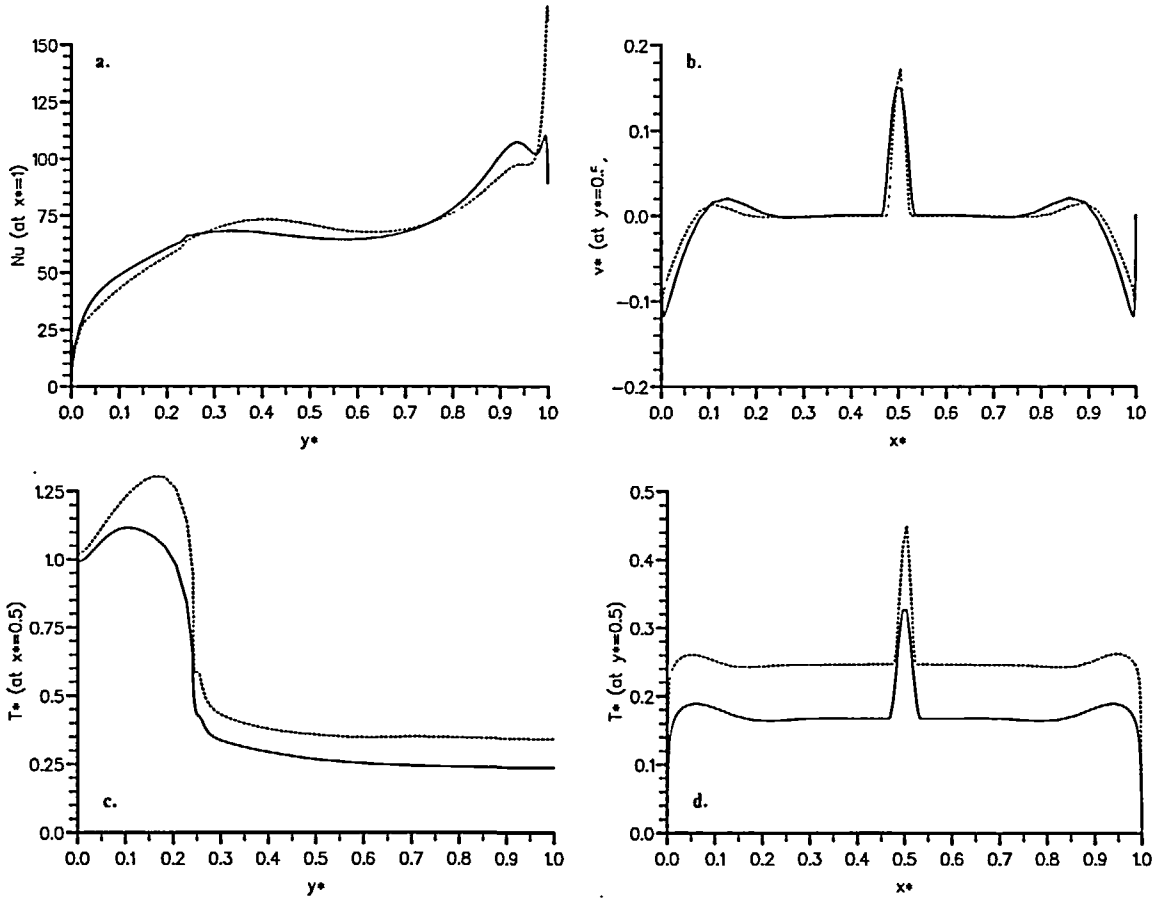

Figure 10 *Case 3b* Local Nusselt number at $x^*=1$ (a) and non-dimensional vertical velocity at $y^*=0.5$ (b) and temperature distribution at $x^*=0.5$ (c) and $y^*=0.5$ (d), using the SWF model (solid line) and the FLB model (dashed line); 90×90 grid

be considered. Turbulence is modelled by means of two-equation k-ε turbulence models, using wall functions or taking low-Reynolds number effects into account.

Three different cases, which give four different flow structures, have been studied using different boundary conditions. The influence of the number of grid points and the grid concentration factors on the numerical solution has been pointed out. In some cases the QUICK scheme has been used and, for the grid densities tested, yields slightly better predictions than the EDS scheme. A comparison between different k-ε turbulence models has also been reported.

Except for the *Case 1b* (differentially heated tall cavity), similar numerical results have been obtained with the SWF and ST models. In comparison with the low-Reynolds number turbulence models tested, significantly higher heat transfer rates have been obtained with the SWF and ST models while closer predictions are obtained for velocity profiles. For the *Case 1a* (differentially heated square cavity), when the grid is refined a delay in the transition point to turbulent flow in the vertical boundary layers is produced and strongly grid-dependent solutions have been obtained. For this case and *Case 2a* (differentilly heated square cavity with inlet and outlet fluid ports), some low-Reynolds-number turbulence models collapse turbulence giving a laminar solution. For the *Case 1b* the IL model, which introduces the empirical YAP correction term

and the GGDH in the well-known LS model, gives the best predictions in comparison to the experimental data. For the *Case 3* (square cavity with an internal heat source), stable convergent numerical solutions have been obtained with the SWF, ST and FLB models, while no stable convergence but an oscillatory behaviour has been obtained with the LS, IL and CH models. In the near future, a transitory analysis for *Case 3* will be necessary to obtain a better knowledge of the physical problem. More experimental work is also required to discern the discrepancies between the different turbulence models.

ACKNOWLEDGEMENTS

This study has been reported by the *Dirección General de Investigación Centifica y Técnica*, Spain, (ref. no. PB90-0606).

REFERENCES

1 Kumar, R. and Yuan, T. D. Recirculating mixed convection flows in rectangular cavities, *J. Thermophysics*, **3**, 321–329 (1989)
2 Papanicolau, E. and Jaluria, Y. J. Mixed convection from an isolated heat source in a rectangular enclosure, *Numerical Heat Transfer*, **18A**, 427–461 (1990)
3 Kelkar, K. M. and Patankar, S. V. Numerical prediction of natural convection in square partitioned enclosures, *Numerical Heat Transfer*, **17A**, 269–285 (1990)
4 Fu, W. S., Perng, J. C. and Shieh, W. J. Transient laminar natural convection in an enclosure partitioned by an adiabatic baffle, *Numerical Heat Transfer*, **16A**, 325–350 (1989)
5 Yucel, A. and Charya, S. Natural convection of a radiating fluid in a partially divided square enclosure, *Numerical Heat Transfer*, **19A**, 471–485 (1991)
6 Rieder, W. and Delfanian, F. Simulation of airborne pollutant levels and infiltration flows in an enclosure, *Journal of Heat Transfer*, **113**, 236–243 (1991)
7 Haghighat, F., Jiang, Z., Wang, J. C. Y. and Allard, F. Air movement in buildings using computational fluid dynamics, *Journal of Heat Transfer*, **114**, 84–92 (1992)
8 Davidson, L. Ventilation by displacement in a three-dimensional room: a numerical study, *Bldg. Environ.*, **24**, 363–372 (1989)
9 Fraikin, M. P., Portier, J. J. and Fraikin, C. J. Application of a k-ε turbulence model to an enclosed buoyancy driven recirculating flow, *ASME Technical Paper*, **80-HT-68** (1980)
10 Henkes, R. A. W. and Hoogendoorn, C. J. Comparison of the standard case for turbulent natural convection in a square enclosure, *Turbulent Natural Convection in Enclosures. A Computational and Experimental Benchmark Study*, Ed. R. A. W. M. Henkes and C. J. Hoogendoorn, *Proc. of the Eurotherm Seminar no. 22*, Delft, 185–213 (1992)
11 Jones, W. P. and Launder, B. E. The prediction of laminarization with a two-equation model of turbulence, *Int. J. Heat and Mass Transfer*, **15**, 301–314 (1972)
12 Launder, B. E. and Sharma, B. I. Application of the energy-dissipation model of turbulence to the calculation of flow near a spinning disc, *Letter in Heat Mass Transfer*, **1**, 131–138 (1974)
13 Hoffman, G. H. Improved form of the low Reynolds number k-ε turbulence model, *Physics Fluids*, **18**, 309–312 (1975)
14 Reynolds, W. C. Computation of turbulent flows, *Ann. Rev. Fluid Mech.*, **8**, 183–208 (1976)
15 Hassid, S., Poreh, M. A turbulent energy dissipation models for flows with drag reduction, *J. Fluids Engng.*, **100**, 107–112 (1978)
16 Lam, C. K. G. and Bremhorst, K. A. A modified form of the k-ε model for predicting wall turbulence, *Journal of Fluid Engng.*, **103**, 456–460 (1981)
17 Dutoya, D. and Michard, P. A program for calculating boundary layers along compressors and turbine blades, *Num. Meth. in Heat Transfer*, ed. R. W. Lewis, Wiley, New York (1981)
18 Chien, K. Y. Prediction of channel and boundary layer flows with a low Reynolds number turbulence model, *AIAA Journal*, **20**, 33–38 (1982)
19 To, W. M. and Humphrey, J. A. C. Numerical simulation of buoyant, turbulent flow—I. Free convection along a heated vertical flat plate, *Int. J. Heat Mass Transfer*, **29**, 573–592 (1986)
20 Nagano, Y. and Hishida, M. Improved form of the k-ε model turbulent shear flows, *J. Fluid Engng.*, **109**, 156–160 (1987)
21 Ince, N. Z. and Launder, B. E. Computation of turbulent natural convection in closed rectangular cavities, *2nd U.K. Nat. Conf. on Heat Transfer*, **2**, 1389–1400 (1988)
22 Davidson, L. Calculation of the turbulent buoyancy driven flow in a rectangular cavity using an efficient solver and two different low Reynolds number k-ε turbulence models, *Numerical Heat Transfer*, **18**, 129–147 (1990)
23 Nagano, Y. and Tagawa, M. An improved k-ε model for boundary layer flows, *J. Fluid Engng.*, **112**, 33–39 (1990)

24 Fan, S., Lakshminarayana, B. and Barnett, M. Low-Reynolds-number k-ε model for unsteady turbulent boundary-layer flows, *AAIA Journal*, **31**, 1777–1784 (1993)
25 Raithby, G. D., Galpin, P. F. and Van Doormaal, J. P. Prediction of heat and fluid flow in complex geometries using general orthogonal coordinates, *Numerical Heat Transfer*, **9**, 125–142 (1986)
26 Leonard, B. P. A stable and accurate convective modelling procedure based on quadratic upstream interpolation, *Comput. Meth. Appl. Mech. Eng.*, **19** (1979)
27 Van Doormaal, J. P. and Raithby, G. D. An evaluation of the segregated approach for predicting incompressible fluid flows, *ASME Paper*, **85-HT-9** (1985)
28 Schneider, G. E. and Zedan, M. A modified strongly implicit procedure for the numerical solution of field problems, *Numerical Heat Transfer*, **4**, 1–9 (1981)
29 Perez Segarra, C. D., Oliva, A., Schweiger, H. and Costa, M. Numerical evaluation of natural and forced convection heat transfer in transparent insulation wall systems, *Sixth International Meeting on Transparent Insulation Technology*, ed. L. F. Jesch, Birmingham, 70–73 (1993)
30 Paolucci, S. Direct numerical simulation of the differentially heated cavity, *Turbulent Natural Convection in Enclosures. A Computational and Experimental Benchmark Study*, Ed. R. A. W. M. Henkes and C. J. Hoogendoorn, *Proc. Eurotherm Seminar no. 22*, Delft, 147–164 (1992)
31 Perez Segarra, C. D., Oliva, A. and Costa, M. Benchmark of turbulent natural convection in a square cavity. Comparison between different k-ε turbulence models, *Turbulent Natural Convection in Enclosures. A Computational and Experimental Benchmark Study*, Ed. R. A. W. M. Henkes and C. J. Hoogendoorn, *Proc. Eurotherm Seminar no. 22*, Delft, 109–120 (1992)
32 Henkes, R. A. W. M. and Hoogendoorn, C. J. Rayleigh-number, aspect-ratio and Prandtl-number dependence for turbulent natural convection in side-heated cavities, *Turbulent Natural Convection in Enclosures. A Computational and Experimental Benchmark Study*, Ed. R. A. W. M. Henkes and C. J. Hoogendoor, *Proc. Eurotherm Seminar no. 22*, Delft, 257–276 (1992)
33 Daffa'alla, A. A. and Betts, P. L. *Experimental Study for Turbulent Natural Convection in a Tall Air Cavity*, Report TFD/91/6, UMIST, UK (1991)